

# Gravitational waves from non-abelian gauge fields at a tachyonic transition

Anders Tranberg,<sup>a</sup> Sara Tähtinen,<sup>b</sup> David J. Weir,<sup>b</sup>

<sup>a</sup>Faculty of Science and Technology, University of Stavanger,  
N-4036 Stavanger, Norway

<sup>b</sup>Department of Physics and Helsinki Institute of Physics,  
P.O. Box 64, FI-00014 University of Helsinki, Finland

E-mail: [anders.tranberg@uis.no](mailto:anders.tranberg@uis.no), [sara.tahtinen@helsinki.fi](mailto:sara.tahtinen@helsinki.fi), [david.weir@helsinki.fi](mailto:david.weir@helsinki.fi)

**Abstract.** We compute numerically the gravitational wave spectrum from a tachyonic preheating transition of a Standard Model-like SU(2)-Higgs system. We find two peaks corresponding to the Higgs and gauge field mass, respectively. The peak magnitude of the spectrum with and without gauge fields is similar, but the gauge fields lead to a further suppression of the gravitational wave signal in the IR region. The far IR is expected to be the relevant range for observations, and so we confirm that a tachyonic transition in the early Universe will not be detectable by LISA, also when involving non-abelian gauge fields.

**Keywords:** Cosmological phase transitions, Primordial gravitational waves (theory)

---

## Contents

<b>1</b>	<b>Introduction</b>	<b>1</b>
<b>2</b>	<b>The SU(2)-scalar model</b>	<b>3</b>
2.1	Reduced models	4
2.2	Initial conditions	4
2.3	Observables and Energy-Momentum tensor	5
<b>3</b>	<b>Gravitational wave production</b>	<b>6</b>
<b>4</b>	<b>Results</b>	<b>7</b>
4.1	Energy distribution and total gravitational wave power	7
4.2	Gravitational wave spectrum	8
4.3	Varying $\lambda$	10
<b>5</b>	<b>Discussion and conclusion</b>	<b>10</b>

---

## 1 Introduction

The ground-breaking direct detection of gravitational waves [1] gives promise that cosmological sources may also be detectable in the foreseeable future. One mission with scope to look for such sources is LISA, due for launch in 2034 [2]. The primary contenders for detection are gravitational waves from inflation and reheating (see for instance [3]), from cosmic defects (see for instance [4]) and from bubble collisions at a first order phase transition (see for instance [5]). The latter can in turn be connected to the creation of the cosmological baryon asymmetry if the phase transition in question is the electroweak one, at a temperature of around 100 GeV.

These processes are favoured observationally by LISA, because the scale of the dynamics is not necessarily set by the microscopic properties of the system, such as particle masses. The long-wavelength behaviour of a system can play a significant role as well. For a first-order phase transition, this might correspond to the radius of bubbles of the new phase, which may grow to near-horizon scales. In preheating, infrared modes are very highly populated. Similarly, cosmic strings potentially extend to the horizon and beyond and could give observable signals. In any case, frequencies corresponding to electroweak mass-scales in the early Universe are much too high to be detectable by LISA, even when redshifted to the present epoch.

For all these different phenomena, numerical simulations are employed to compute the spectrum and strength of the gravitational wave signal, sourced by inhomogeneous, non-perturbative field dynamics [6–14]. Reheating at the end of inflation is typically modelled by one or more (self-)interacting scalar fields, which may or may not be coupled to gauge fields. For baryogenesis at a first order thermal phase transition, multiple fields are in play, but from the point of view of gravitational wave creation, these are likely well modelled by an ambient fluid, interacting with the Higgs field wall [8, 15].

In hybrid inflation models, the inflaton  $\sigma$  is coupled to a second field  $\phi$ , which undergoes a symmetry breaking transition as the inflaton field slow-rolls past some critical value. The

dynamics of the second field in turn triggers the end of inflation by effectively changing the inflaton potential and ending the slow-roll stage. The combined dynamics of the two fields can subsequently be quite complicated, with the possibility of resonant particle production. However, in the simplest case the second field simply performs a symmetry breaking “roll-off” at zero temperature, from zero value at the top of a negative-curvature potential. Writing for future convenience in terms of a complex scalar, we have for the second field  $\phi$

$$V(\phi) = V_0 + \mu_{\text{eff}}^2(t)\phi^\dagger\phi + \lambda(\phi^\dagger\phi)^2, \quad (1.1)$$

where  $\mu_{\text{eff}}^2(t)$  is a model-dependent function of time (given by the motion of the inflaton field, say). It is assumed to evolve from being positive to being negative, thereby triggering the symmetry breaking transition. We can model it as<sup>1</sup>

$$\mu_{\text{eff}}^2(t) = \mu^2 \left(1 - \frac{2t}{\tau_q}\right), \quad u = -\frac{1}{2\mu^3} \frac{d\mu_{\text{eff}}^2(t)}{dt} \Big|_{\mu_{\text{eff}}=0} = \frac{1}{\mu\tau_q}. \quad (1.2)$$

Matching to, for instance, a quartic “portal” coupling model, we could imagine writing

$$\mu_{\text{eff}}^2(t) = (\xi^2\sigma^2 - \mu^2), \quad u = -\frac{1}{2\mu^3} \frac{d\mu_{\text{eff}}^2(t)}{dt} \Big|_{\mu_{\text{eff}}=0} = -\frac{\xi\dot{\sigma}_c}{\mu^2}, \quad (1.3)$$

so that  $\tau_q \simeq -\mu/\xi\dot{\sigma}_c$ , where the subscript  $c$  refers to the time of the quench  $\sigma_c = \mu/\xi$ .

Such a transition results in exponentially growing field modes with  $|\mathbf{k}| \leq \mu$ , and is known as a spinodal decomposition or tachyonic preheating [16]. The subsequent redistribution of the initial potential energy in  $V_0$  is a highly effective preheating mechanism. In a given model, the additional kinetic energy of the inflaton field, and possible resonances (resonant preheating) must be considered.

The process of preheating through a spinodal transition is a violent and inhomogeneous process, and produces gravitational waves [17]. These could potentially be within the frequency range of LISA, even though the characteristic scales of the transition (typically  $\mu$  and  $\tau_q$ ), are of the order of a GeV or more. This is because the exponential growth applies to all modes far into the IR, and hence in principle all the way to the horizon scale.

Previous simulations of scalar fields only [12, 14] have shown that gravitational waves are indeed produced in such a transition, but that the spectrum tends to peak around the scale of the particle masses. To the IR of this peak, there is first a  $\propto k$  behaviour and then  $\propto k^3$ . This in spite of there being high occupation numbers in the field modes all the way to  $k = 0$ . For scalar fields, this is perhaps not unexpected given the form of the relevant source term (see below), but still disappointing. However, since these models are not directly connected to known physics (such as the Standard Model), there is some freedom in choosing the couplings and energy scale, including the quench speed  $u$ . In this way, one may construct models whose signal approaches the LISA-detectable region.

Whereas the inflaton is expected to be a gauge singlet, the second field  $\phi$  need not be. Guided by the situation in the Standard Model, it is natural to expect both abelian (U(1)) and non-abelian (SU( $N$ )) gauge fields to couple to such a “Higgs” field, and participate in the preheating mechanism. One may even entertain the notion that the second field *is* the Standard Model Higgs field. In this case, a fast spinodal transition from zero temperature (for instance at the end of low-scale inflation), may be responsible for the baryon asymmetry of the Universe [18–21].

---

<sup>1</sup>Our quench speed  $u$  is equivalent to the quantity  $V_c$  in [17].

Previous simulations of gravitational waves from tachyonic preheating consider only the case where the gauge group is abelian [6]. In that case, new sources of gravitational waves appear, but again the peak of the spectrum stays in the UV, corresponding to the particle masses (scalar and gauge). Again, some freedom in the choice of parameters means it is possible to shift the peak amplitude and position towards the LISA detection region. Interesting considerations arise in this context from the possible generation of cosmic strings, which have been seen to alter, and give additional features to, the power spectrum of gravitational waves.

Non-abelian fields self-interact strongly, and provide their own contribution to the gravitational wave source, a contribution which a priori could be significant. In the present work we will compute the spectrum of gravitational waves, as a function of the mass scale  $\mu$  and the quench time  $\tau_q$ . For most of our simulations, we will be conservative and assume a Standard Model-like theory, by setting the Higgs and gauge (self-)interaction couplings  $\lambda$  and  $g^2$  equal to their Standard Model values. Hence, when the scale  $\mu$  is around 100 GeV, our results apply directly to a Standard Model transition. When  $\mu \gg 100$  GeV, the theory is a specific realisation of a generic SU(2)-Higgs system.

The paper is structured as follows: In the next Section, we will present our model, important considerations and observables of interest. In Section 3 we set out our numerical procedure and definitions to compute the gravitational wave spectrum. In Section 4 we consider basic numerical observables, including components of the energy-momentum tensor, as well as the total energy generated in gravitational waves. We also present the full spectrum of gravitational waves, and analyse new features and contrast them with a scalar-only theory. We conclude in Section 5, where we also provide the extrapolation of the spectrum to the present day, and consider the potential for detection by LISA.

## 2 The SU(2)-scalar model

We consider a complex scalar doublet  $\phi$  (four real components), coupled to an SU(2) gauge field  $A_\mu$ . We have the action:

$$S = - \int d^4x \left\{ \frac{1}{4g^2} F^{a,\mu\nu} F_{a,\mu\nu} + \left[ (D_\mu \phi)^\dagger D^\mu \phi + \mu_{\text{eff}}^2(t) \phi^\dagger \phi + \lambda (\phi^\dagger \phi)^2 \right] \right\}, \quad (2.1)$$

where

$$F_{\mu\nu}^a = \partial_\mu A_\nu^a - \partial_\nu A_\mu^a + \epsilon^{abc} A_\mu^b A_\nu^c, \quad (2.2)$$

$$D_\mu \phi = (\partial_\mu - i A_\mu^a \tau^a) \phi. \quad (2.3)$$

and  $\mu_{\text{eff}}^2(t)$  is given by Eq. (1.2). The scalar field components are

$$\phi = \frac{1}{\sqrt{2}} \begin{pmatrix} \phi_2 + i\phi_3 \\ \phi_0 + i\phi_1 \end{pmatrix}. \quad (2.4)$$

In the following, we will refer to the scalar as the Higgs field. Although we may only identify it with the Standard Model Higgs in the case where  $\mu \simeq 100$  GeV, for any energy scale the symmetry breaking transition will lead to an analogue of the Higgs mechanism for the gauge fields coupled to it. In line with this terminology, we speak of the Higgs mass  $m_H = \sqrt{2}\mu$ , the Higgs expectation value  $v = \mu/\sqrt{\lambda}$  and the W-mass (for the gauge fields),  $m_W = gv/2$ . We will take the Standard Model values from  $m_H = 125$  GeV,  $m_W = 80.2$  GeV, giving  $\lambda \simeq 0.13$  and  $g \simeq 0.65$ . These we will keep fixed while varying  $\mu^2$  (and as a result,  $v$ ). We will also

briefly discuss varying  $\lambda$  (we consider  $\lambda = 0.001$  and  $\lambda = 0.01$ ), leaving the other parameters fixed. The lattice spacing will be fixed by  $a\mu = 0.17$ , with a lattice size of  $N^3 = 384^3$  sites.

From the classical action (2.1), we can by variation with respect to  $\phi$  and  $A_\mu$  derive the classical equations of motion. These are explicit, coupled, non-linear, partial differential equations that can be solved by discretisation on a spatial cubic grid, and then evolved in time. We follow the standard procedure to do this (see, for instance [22]).

In a cosmological context, we should in principle include the expansion of the Universe through an FRW metric in the action. However, we know that the timescales involved are of the order of  $10^2 \mu^{-1}$ , the total energy density is  $V_0 = \mu^4/(4\lambda)$  and so we can ignore Hubble expansion as long as

$$1 \gg \frac{100H}{\mu} = 100\sqrt{\frac{1}{12\lambda}} \frac{\mu}{M_{\text{p}}}. \quad (2.5)$$

Energy scales  $\mu \lesssim 10^{13}$  GeV satisfy this bound for our choices of  $\lambda$ .

## 2.1 Reduced models

We are mainly interested in the effect of including a non-abelian gauge field in the dynamics, and so for comparison, we consider two other models, one with a complex (or two real) scalar fields and one with the complex doublet<sup>2</sup>, but no gauge field (essentially an  $O(4)$ -model). The actions are correspondingly for the singlet (denoted by the label “2”)

$$S_2 = - \int d^4x [(\partial_\mu \phi)^* \partial^\mu \phi + \mu_{\text{eff}}^2(t) \phi^* \phi + \lambda(\phi^* \phi)^2], \quad (2.6)$$

and for the doublet (denoted by the label “4”).

$$S_4 = - \int d^4x [(\partial_\mu \phi)^\dagger \partial^\mu \phi + \mu_{\text{eff}}^2(t) \phi^\dagger \phi + \lambda(\phi^\dagger \phi)^2]. \quad (2.7)$$

Although in the following we describe the implementation and observables for the SU(2)-Higgs model (denoted by the label “4+G”), these all apply with trivial adaptations to the complex singlet and complex doublet case.

## 2.2 Initial conditions

We will model the cold spinodal transition by assuming that the initial state is the vacuum in the potential

$$V_{\text{in}}(\phi) = \mu^2 \phi^\dagger \phi, \quad (2.8)$$

so that the (free) modes of the Higgs field obey

$$\langle \phi_a(k) \phi_b(k)^\dagger \rangle = \frac{1}{2\sqrt{\mu^2 + k^2}} \delta_{ab}, \quad \langle \pi_a(k) \pi_b(k)^\dagger \rangle = \frac{1}{2} \sqrt{\mu^2 + k^2} \delta_{ab}. \quad (2.9)$$

with  $a$  denoting the four (two) real scalar degrees of freedom. We only initialise unstable modes with  $|\mathbf{k}| < \mu$ . These are the ones that grow large and subsequently validate the use

---

<sup>2</sup>Simulations with a single real field were found to exhibit lattice artefacts to do with domain walls stretching through the lattice. This is interesting, but not relevant for us here.

of classical dynamics rather than full quantum dynamics. Careful discussions of this point can be found in Refs. [23–25]. Consistent with this way of thinking, all the gauge fields will be put to zero initially  $A_\mu = 0$ . Throughout, we will evolve the equations in temporal gauge  $A_0 = 0$ . We also initialise the gauge field conjugate momenta  $E_i$  to zero. There is therefore an insignificant residual per-site violation of the Gauss law of  $10^{-8}$ .

These initial conditions are closely related to those of Ref. [6]. However, we note that although one may classically scale out the quantity  $v$  from the classical equations of motion for the scalar, one cannot in the same way rescale the quantum initial conditions. These are the same for any choice of  $v$ , provided  $\mu$  is fixed. On the lattice they are determined by the choice of lattice scale. Hence, one may not trivially scale the results from one value of  $v$  to another, since the initial condition is then de facto different (although the resulting error is probably small). On the other hand, one may compute dimensionless ratios at a given lattice spacing (defined for instance in units of the mass  $a\mu$ ), and then rescale trivially in  $\mu$ . We will do this below.

### 2.3 Observables and Energy-Momentum tensor

The energy-momentum tensor of the theory follows from variation with respect to the metric. For the scalar field, we have for the energy density

$$\rho_\phi = (\partial_t \phi)^\dagger \partial_t \phi + (D_i \phi)^\dagger D_i \phi + \mu_{\text{eff}}^2(t) \phi^\dagger \phi + \lambda(\phi^\dagger \phi)^2 + V_0. \quad (2.10)$$

We may further subdivide this contribution into a kinetic (first term), gradient (second term) and potential part (the rest). Initially, the bulk of the energy is in  $V_0$ . An important consequence of our quench mechanism is that total energy is not conserved, because  $\mu_{\text{eff}}^2(t)$  has an explicit time-dependence. We have that

$$\frac{dE}{dt} = \frac{d\mu_{\text{eff}}^2(t)}{dt} \int \phi^\dagger \phi(\mathbf{x}, t) d^3 \mathbf{x}. \quad (2.11)$$

For the largest quench times presented here, this leads to a sizeable depletion of energy of up to 75%, or reduction of the final temperature of 50 %. This is the price we pay for simplifying the system by ignoring the specific and model-dependent dynamics of the trigger (inflaton) field.

It turns out [26], that such a quench, where energy is initially taken out of the Higgs field, corresponds to a particular parameter subspace of the model given in Eq. (1.3). At later times, energy is reintroduced as the system equipartitions and equilibrates. The time-scale for this to complete is much longer than the time-scales considered here. The late-time dynamics can also generate gravitational waves (see for instance [6]).

Gravitational waves are sourced by the off-diagonal spatial components  $T_{ij}^\phi$ , given by

$$T_{ij}^\phi = (D_i \phi)^\dagger (D_j \phi) + (D_i \phi)(D_j \phi)^\dagger = 2\text{Re} \left[ (D_i \phi)^\dagger (D_j \phi) \right]. \quad (2.12)$$

For the gauge field, we have

$$T_{\mu\nu}^A = \eta_{\mu\nu} \mathcal{L} - \frac{1}{g^2} \eta^{\alpha\beta} F_{\mu\alpha}^a F_{\nu\beta}^a. \quad (2.13)$$

The energy density is

$$\rho_A = \frac{1}{g^2} \left( F_{0\alpha}^a F_{0\alpha}^a + \frac{1}{4} F^{a,\mu\nu} F_{a,\mu\nu} \right) = \frac{1}{2} (E_i^2 + B_i^2). \quad (2.14)$$

The off-diagonal spatial components entering the gravitational wave computation is then

$$T_{ij}^A = -\frac{1}{g^2} F_i^{\beta,a} F_{j\beta}^a. \quad (2.15)$$

The complex singlet and doublet models for comparison have no gauge field contribution, and the scalar energy-momentum expressions include normal instead of covariant derivatives, with two and four real fields, respectively.

### 3 Gravitational wave production

Given the background scalar-gauge field theory simulation, from which we extract the energy-momentum tensor as described above, we can compute the gravitational wave spectrum as described in the following. For a more detailed exposition we refer to Ref. [9], and references therein. At each step of the simulation we compute the parts of the stress energy tensor that source metric perturbations, namely  $T_{ij}^A$  for the gauge field and  $T_{ij}^\phi$  for the Higgs field. We can then numerically explicitly solve the wave equation for the metric perturbation  $u_{ij}$ ,

$$\ddot{u}_{ij} - \nabla^2 u_{ij} = 16\pi G (T_{ij}^\phi + T_{ij}^A). \quad (3.1)$$

Going to momentum space

$$u_{ij}(\mathbf{k}) = \int d^3\mathbf{x} u_{ij}(\mathbf{x}) e^{-i\mathbf{k}\cdot\mathbf{x}}, \quad (3.2)$$

we can then project out the propagating, transverse-traceless degrees of freedom

$$h_{ij}(t, \mathbf{k}) = \lambda_{ij,lm}(\hat{\mathbf{k}}) u_{lm}(t, \mathbf{k}), \quad (3.3)$$

where

$$\lambda_{ij,lm}(\mathbf{k}) = P_{ik}(\mathbf{k}) P_{jl}(\mathbf{k}) - \frac{1}{2} P_{ij}(\mathbf{k}) P_{kl}(\mathbf{k}), \quad P_{ij}(\mathbf{k}) = \delta_{ij} - \frac{k_i k_j}{|\mathbf{k}|^2}. \quad (3.4)$$

We can then construct the total energy density in the gravitational waves

$$\rho_{\text{GW}} = \frac{1}{32\pi G V} \int \frac{d^3\mathbf{k}}{(2\pi)^3} \langle \dot{h}^{ij}(\mathbf{k}) \dot{h}^{ij}(-\mathbf{k}) \rangle, \quad (3.5)$$

where the average is to be taken over the full quantum state, or in practice an ensemble of realisations of the field theory initial conditions. We may also define the spectrum of gravitational waves,

$$\frac{d\rho_{\text{GW}}}{d \ln k} = \frac{1}{32\pi G V} \frac{k^3}{(2\pi)^3} \int d\Omega \langle \dot{h}^{ij}(\mathbf{k}) \dot{h}^{ij}(-\mathbf{k}) \rangle, \quad (3.6)$$

where the integral is now only over solid angle. The spectrum is then a function of the length of  $\mathbf{k}$  only. Note the contraction of labels  $ij$  in Eqs. (3.5) and (3.6).

We solve Eq. (3.1) in parallel as the simulation of the (gauge-)Higgs system is performed. The source terms are time-dependent, and are in effect integrated over time to produce the final gravitational wave spectrum, and the total energy density in gravitational waves. This energy density is numerically completely negligible relative to the total energy density of the field theory system, and it makes little sense feeding the created gravitational waves back into the field theory simulation. Hence the gravitational waves are computed in the background of the (gauge-)Higgs system with no back-reaction. Ultimately, it is the quantity given by Eq. (3.6) that may be inferred from observations, suitably transported from the end of inflation to the present time. We will postpone the conversion to the present time to Section 5.

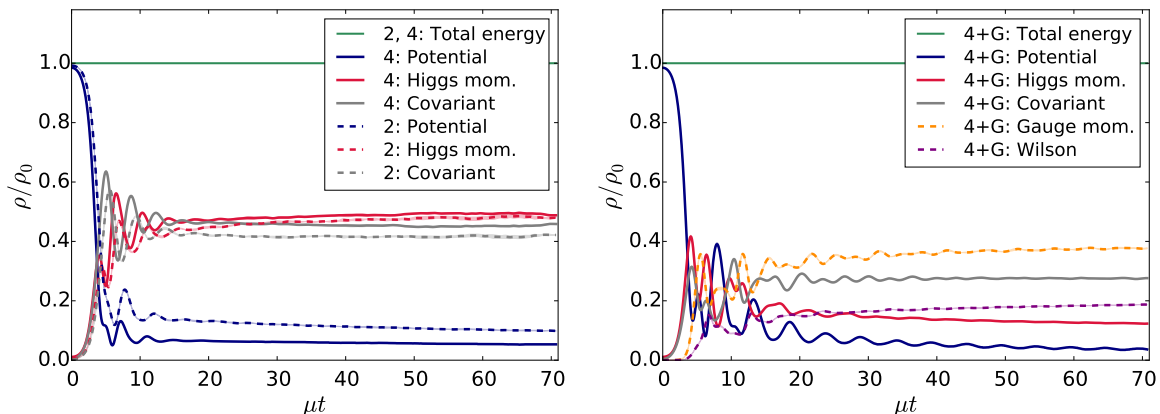


**Figure 1.** The energy components of the complex singlet and doublet scalar systems (left) and the gauge-doublet system (right). Quench time is  $\mu\tau_q = 0$ .

## 4 Results

### 4.1 Energy distribution and total gravitational wave power

Gravitational waves are sourced by the off-diagonal components of the energy-momentum tensor, but it is instructive to consider the energy density and its components, to track where the energy goes. Initially, all the energy, except for small fluctuations in the Higgs field, is in the Higgs potential  $V_0$ . In the tachyonic transition, the low momentum modes  $|\mathbf{k}| < \mu$  grow exponentially, picking up kinetic energy and gradient energy, while losing potential energy. With gauge fields coupled to it, these will also grow exponentially, and reheat simultaneously [27].

In Fig. 1, we show the various energy components for a simulation at one particular quench time  $\mu\tau_q = 0$ . On the left, we show simulations with a complex scalar (2, dashed lines) and a complex doublet (4, full lines). We see that the potential energy is transferred to kinetic and gradient energy within a few units of  $\mu^{-1}$ . There is some quantitative difference between the singlet and doublet case, but qualitatively, it is the same. The transition is over after  $\mu t \simeq 15$ . Note that for zero quench time, no energy is lost because of the quenching process (2.11).

On the right-hand panel of the figure, we see that including the gauge field changes the situation. Although the potential energy is released very quickly as for the pure-scalar cases, this transfer only completes somewhat later. The Higgs field oscillates more and for longer and has a smaller fraction of the total energy. Some of this energy is instead transferred to the gauge field, which takes longer to be excited and settle, lasting until  $\mu t \simeq 20 - 25$ . A detailed analysis of this preheating process can be found in [27, 28]. The main features are that there is a short, violent roll-of period, followed by kinetic equilibration (and equipartition) as the self-interactions kick in, with a time-scale of a few hundreds in mass units. A Bose-Einstein like particle spectrum is created with a sizeable effective chemical potential which disappears on a time-scale of a few thousands in mass units, through chemical equilibration.

In Fig. 2 (left), we show the total energy in gravitational waves from gauge-scalar simulations for five different quench times. The energy density is normalised to the initial energy in the Higgs potential, and with a prefactor  $\mu^2/M_p^2$ , with  $M_p$  the Planck mass. For

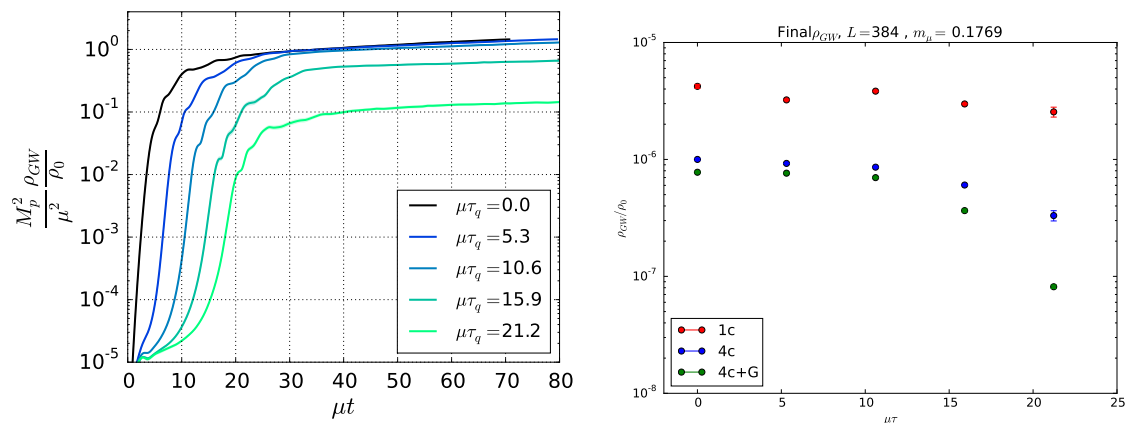


**Figure 2.** The total gravitational wave energy density for the gauge-doublet models for five quench times (left). And the final value, for all quench times and models (right).

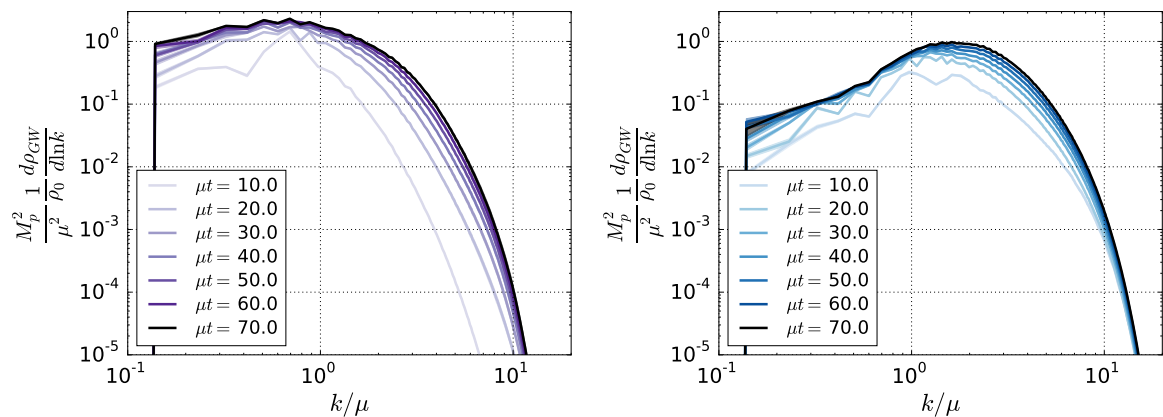


**Figure 3.** The power spectrum for a singlet (left) and gauge-doublet system (right) for different times. Quench time is  $\mu\tau_q = 0$ .

a given value of  $\mu$ , one should therefore rescale the curves in the plot accordingly. As an example, the Standard Model has  $\mu \simeq 88$  GeV, giving a prefactor of  $1.3 \times 10^{-33}$ .

We see that the violent transition causes the gravitational energy to grow exponentially until a time  $\mu t \simeq 10$  after the quench, and that it continues to grow slowly afterwards. We also see that the final total power at first has little dependence on quench time, and then decreases with quench time. This shows that when the time-scale of the quench is below a certain cut-off, the time-scale of the dynamics is the spinodal roll-off itself. In Fig. 2 (right) we show the total gravitational wave energy for all three models, for all quench times. Only once  $\mu\tau_q > 10$  does the GW energy start decreasing, and most for the gauge-scalar system. The gravitational wave energy is generically larger for scalar-only models.

## 4.2 Gravitational wave spectrum

Having found the total power in gravitational waves and its dependence on quench time, we now proceed to break this up in a whole spectrum of gravitational waves. In Fig. 3, we show the spectra for different times for quench time  $\mu\tau_q = 0$  for a complex singlet (left) and a

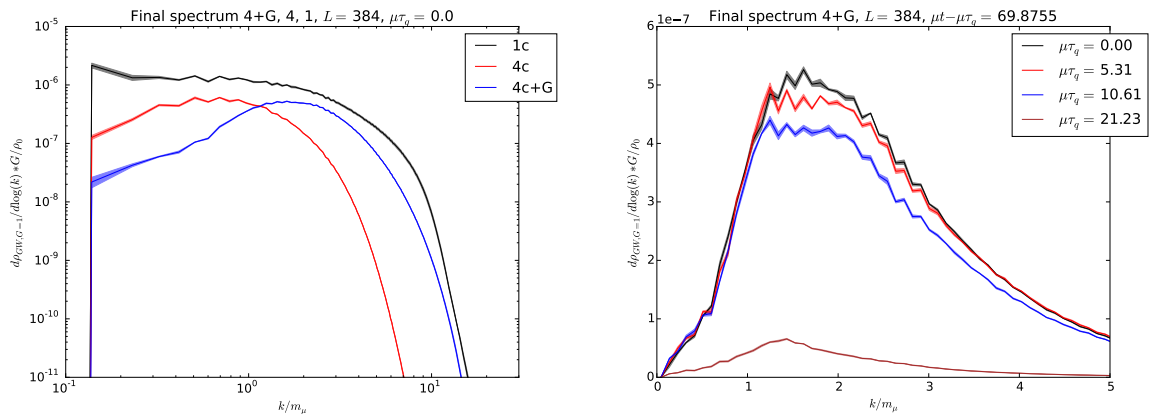


**Figure 4.** The final spectrum for the singlet, doublet and gauge-doublet system at zero quench time (left). And for the gauge-scalar case, for different quench times (right)

doublet with a gauge field (right). We have again multiplied by a factor of  $M_{\text{p}}^2/\mu^2$ , to be scaled back once a value for  $\mu$  is chosen. The spectrum grows and converges in shape and magnitude at time  $\mu t \simeq 60$ . The maximum value is similar, around 1 – 2, with the peak shifted by a factor of 2 ( $k/\mu \simeq 0.7$  and  $\simeq 1.5$ , respectively). For comparison, we note that the Higgs mass is  $m_H = \sqrt{2}\mu \simeq 1.4\mu$  (once symmetry breaking is completed). And for the gauge field  $m_W = g\mu/2\sqrt{\lambda} \simeq 0.9\mu$ . The unstable modes have momenta up to  $k = \mu$ .

Whereas for the complex singlet this magnitude decreases only slightly as far into the IR as we can cover dynamically, when including gauge fields, the spectrum decreases linearly in the IR. This produces a true peak at  $k/\mu \simeq 1.5$  dropping by an order of magnitude by  $k/\mu = 0.2$ . Deep in the IR, we expect on general grounds a behaviour as  $k^3$ .

In Fig. 4 (left) we show the spectra at the final time of  $\mu t = 70$ . The scalar cases display a maximum at a common  $k/\mu \simeq 0.7$ , whereas the gauge field shifts the peak to  $k/\mu \simeq 1.5$ . The complex singlet case has a slightly higher peak amplitude, by a factor of about 2. We then show the final spectrum for the gauge-doublet case for different quench times (this time on a linear scale) in Fig. 4 (right). We see that peak value decreases monotonically with longer quench time, although again the very quick quenches cannot be resolved by the field dynamics. Note that since gravitational wave production continues in principle indefinitely, we have chosen to compare different quench time results at equal time after the end of the quench,  $\mu t_{\text{final}} = \mu\tau_q + 70$ . The slowest quench has a peak amplitude down by a factor of 8.

Finally, we can attempt an analysis of the peak of the spectrum for the gauge-doublet case, shown in Fig. 5. The peak position varies in the range  $k/\mu = 1.4 - 1.6$  (not shown). The peak amplitude (left-hand plot) show a decreasing trend as a function of quench time, reminiscent of the total energy density in gravitational waves, Fig. 2. One may also attempt a fit of the IR slope(s) of the peak (right-hand plot) to find consistently a power of 1.5 – 1.75 for all quench times on the range  $\mu/2 < k < \mu$ . However, this power law is replaced by a shallower  $k$ -dependence further in the IR,  $k < \mu/2$ . This far-IR power law is in the range 0.8 – 1.1 and generally close to unity. Further still, at scales too large to study in our lattice simulations, this will give way to the causal  $k^3$  power law.

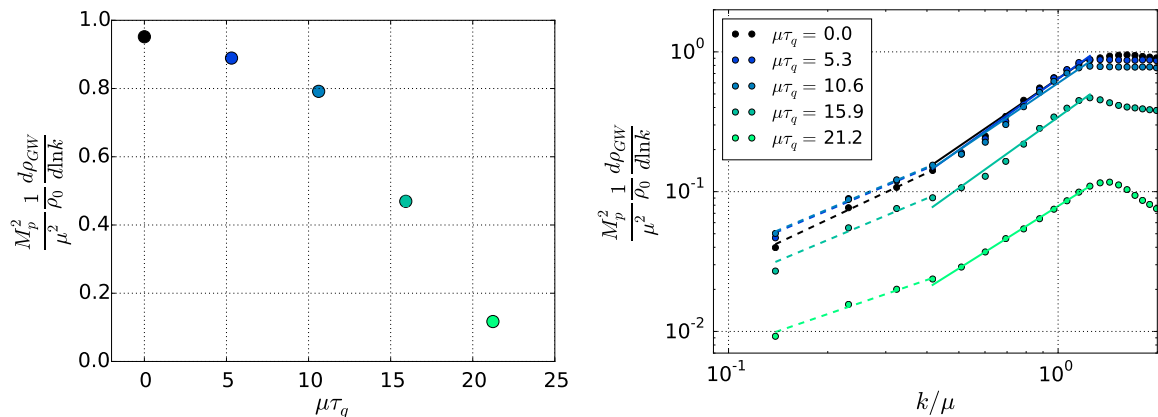


**Figure 5.** The peak amplitude (left) and IR slope (right) as a function of quench time.

### 4.3 Varying $\lambda$

So far, all our simulations have been done with  $\lambda = 0.13$ , the Standard Model value. The Standard Model is special in that the gauge boson and Higgs masses are very similar

$$\frac{m_H}{m_W} = \sqrt{\frac{8\lambda}{g^2}} \simeq 1.57. \quad (4.1)$$

This means that although there are two mass-scales in the problem (in addition to quench time), we only see one peak in the spectrum of gravitational waves.

One way to disentangle the two scales is to make  $\lambda$  (and hence  $m_H/m_W$ ) smaller. We will keep  $\mu$  fixed, and so what changes is  $m_W$  (in physical and lattice units) and the Higgs vev  $v$ . In Fig. 6 (left) we show the spectrum of gravitational waves for four different values of  $\lambda$ , for the gauge-scalar model only. We see that as the gauge boson mass increases ( $\lambda$  decreases) the peak resolves into two distinct peaks. The amplitude also increases significantly, by one or two orders of magnitude.

For  $\lambda = 0.001$ , the W-mass is clearly at the edge of our dynamical range ( $am_W \simeq 7.3 \times am_H$ ), and we can therefore not go to even smaller Higgs coupling. In order to confirm the origin of the second peak, we show in Fig. 6 (right) all three models with  $\lambda = 0.001$ . There is now no trace of the second peak, showing that the gauge field is really responsible (and not, say, the value of  $v$ ). The increase in magnitude as  $\lambda$  is decreased is common for all the models. For smaller  $\lambda$ , the exponential tachyonic instability lasts longer.

Such peak structure and other tell-tale features of multiple mass-scales would be prime targets for observations. However, as the Higgs and W-mass scales are unfortunately far from the observational range of LISA, we will not proceed further with a complete parameter scan of the theory.

## 5 Discussion and conclusion

As mentioned, we take the energy scale  $\mu$  small enough relative to the Planck mass, that we can ignore the expansion of the Universe during the time-scale of the simulation. Then we have the simple relation between a given physical scale on the lattice  $ak$  and the frequency

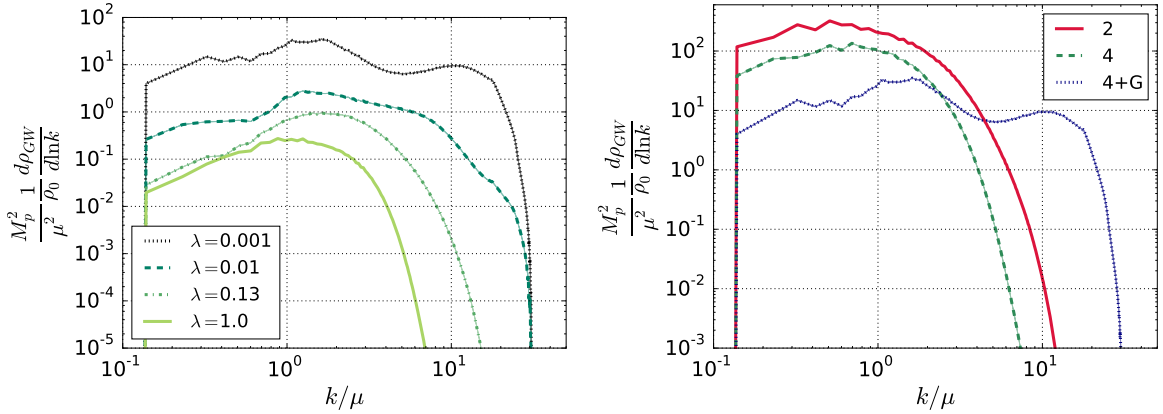


**Figure 6.** The gauge-scalar spectrum for different  $\lambda$  (left), and for  $\lambda = 0.001$  for different models (right).  $\mu\tau_q = 0$ .

$f$  today [14]

$$f = 4 \times 10^{10} \text{ Hz} \left( \frac{ak}{a\rho^{1/4}} \right) = 4 \times 10^{10} \text{ Hz} \left( \frac{k}{\mu} \right) (4\lambda)^{1/4} = 3.4 \times 10^{10} \text{ Hz} \times \frac{k}{\mu}, \quad (5.1)$$

where we have taken the value  $\lambda = 0.13$  (multiply by 0.3 for  $\lambda = 0.001$ ). Hence, for fixed  $\lambda$ , the peak frequency for any choice of  $\mu$  can be read off from the figures. Similarly, the amplitude of the spectrum is given by

$$\Omega_{\text{gw}} h^2 = \frac{1}{\rho} \frac{d\rho_{\text{GW}}}{d \ln k} \left( \frac{g_*}{g_0} \right)^{-1/3} \Omega_{\text{rad}} h^2 = 9.3 \times 10^{-6} \times \frac{1}{\rho} \frac{d\rho_{\text{GW}}}{d \ln k}, \quad (5.2)$$

using  $\Omega_{\text{rad}} h^2 = 4.3 \times 10^{-5}$  and  $g_*/g_0 \simeq 100$ . Again, this amplitude may therefore be read off from the figures, remembering to rescale by  $\mu^2/M_{\text{p}}$ .

The peak sensitivity of the LISA mission is around 0.01 Hz, whereas our maximum signal occurs at  $k/\mu \simeq 1.5$ , corresponding to  $5 \times 10^{10}$  Hz. The peak amplitude is

$$\Omega_{\text{gw}} h^2 = 9.3 \times 10^{-6} \left( \frac{\mu}{M_{\text{p}}} \right)^2, \quad (5.3)$$

which is  $10^{-38}$  for the electroweak scale and  $10^{-12}$  for a GUT-scale transition. This applies to  $\lambda = 0.13$ , and we have seen that a few orders of magnitude can be gained by decreasing  $\lambda$ . Increasing the quench time decreases the magnitude of the gravitational spectrum, once the quench is slower than the finite time-scale off the Higgs roll-off.

When including gauge fields, we observe a stronger suppression in the IR (see also Ref. [6] for the Abelian case) with a power-law slope of about 1.6 near the peak. This gives way to a near-linear dependence further from the peak, although at very long wavelengths the causal behaviour of the source implies a steeper cubic power law. Hence, we expect that the signal 13 decades into the IR will be completely undetectable by LISA.

We saw that varying the coupling  $\lambda$ , a second peak corresponding to the gauge field mass emerges. It is possible that allowing for a very small (or zero) gauge field mass could overcome the IR suppression, by effectively shifting the gauge field peak far into the IR. The

obvious candidate for this is the Standard Model photon but fields with very small masses are difficult to contain on a finite lattice. Also, although the identity of the photon is ambiguous during the tachyonic transition, once the Higgs mechanism is realised, the mass really is zero. There is no parameter with which to gradually “turn the mass off”. We did not implement the photon in our simulations, and postpone a resolution of this issue to future work.

The peak signal frequency depends only on the scale  $\mu$  through the combination  $k/\mu$ , because we assume that the Hubble rate is determined by the Standard Model-inflaton energy component only. If another energy component than the Higgs potential would dominate the expansion of the Universe, the peak would redshift differently. Introducing such a new component, one would have to account for how it decays into SM degrees of freedom prior to BBN.

The hot plasma present in the early universe after reheating is an additional source of gravitational waves [29]. In fact, it might even prove to be a more significant source than the signal predicted for a tachyonic transition. The amplitude of gravitational waves from the plasma would be today (for typical Standard Model values of the energy density and shear viscosity)

$$\Omega_{\text{gw}} h^2 \approx 10^{-6} \left( \frac{T_{\text{max}}}{M_{\text{p}}} \right) \quad (5.4)$$

where  $T_{\text{max}}$  would be the maximum temperature of the plasma, as it forms. This can be parametrically larger than the contribution of Eq. (5.3) by a factor  $M_{\text{p}} T_{\text{max}}/\mu^2$ , with a peak at wavenumber  $k \sim T_0$ , the temperature at which electroweak symmetry breaking takes place. This is in contrast to a first-order phase transition, where such plasma dynamics will be an insignificant source of gravitational waves except at the highest frequencies.

It is not a priori unreasonable to think that the copious production of particles in the IR would allow for detection of a tachyonic transition through gravitational waves. We have however seen that including non-abelian gauge fields further suppresses the signal relative to scalar-only theories. With the possible caveats described above we must conclude that tachyonic preheating will not be observable at LISA.

**Acknowledgments:** AT is supported by a UiS-ToppForsk grant from the University of Stavanger. ST is supported by the Magnus Ehrnrooth foundation and Academy of Finland grant 267842. DJW is supported by Academy of Finland grant 267286. The authors thank Mark Hindmarsh for enlightening discussions. The numerical work was performed on the Abel Cluster, owned by the University of Oslo and the Norwegian metacenter for High Performance Computing (NOTUR), and operated by the Department for Research Computing at USIT, the University of Oslo IT-department.

## References

- [1] B. P. Abbott *et al.* [LIGO Scientific and Virgo Collaborations], Phys. Rev. Lett. **116** (2016) no.6, 061102 doi:10.1103/PhysRevLett.116.061102 [arXiv:1602.03837 [gr-qc]].
- [2] H. Audley *et al.*, arXiv:1702.00786 [astro-ph.IM].
- [3] N. Bartolo *et al.*, JCAP **1612** (2016) no.12, 026 doi:10.1088/1475-7516/2016/12/026 [arXiv:1610.06481 [astro-ph.CO]].
- [4] P. Binetruy, A. Bohe, C. Caprini and J. F. Dufaux, JCAP **1206** (2012) 027 doi:10.1088/1475-7516/2012/06/027 [arXiv:1201.0983 [gr-qc]].

- [5] C. Caprini *et al.*, JCAP **1604** (2016) no.04, 001 doi:10.1088/1475-7516/2016/04/001 [arXiv:1512.06239 [astro-ph.CO]].
- [6] J. F. Dufaux, D. G. Figueroa and J. Garcia-Bellido, Phys. Rev. D **82** (2010) 083518 doi:10.1103/PhysRevD.82.083518 [arXiv:1006.0217 [astro-ph.CO]].
- [7] D. G. Figueroa, M. Hindmarsh and J. Urrestilla, Phys. Rev. Lett. **110** (2013) no.10, 101302 doi:10.1103/PhysRevLett.110.101302 [arXiv:1212.5458 [astro-ph.CO]].
- [8] M. Hindmarsh, S. J. Huber, K. Rummukainen and D. J. Weir, Phys. Rev. Lett. **112** (2014) 041301 doi:10.1103/PhysRevLett.112.041301 [arXiv:1304.2433 [hep-ph]].
- [9] M. Hindmarsh, S. J. Huber, K. Rummukainen and D. J. Weir, Phys. Rev. D **92** (2015) no.12, 123009 doi:10.1103/PhysRevD.92.123009 [arXiv:1504.03291 [astro-ph.CO]].
- [10] D. G. Figueroa, J. Garca-Bellido and F. Torrent, Phys. Rev. D **93** (2016) no.10, 103521 doi:10.1103/PhysRevD.93.103521 [arXiv:1602.03085 [astro-ph.CO]].
- [11] M. Hindmarsh, S. J. Huber, K. Rummukainen and D. J. Weir, arXiv:1704.05871 [astro-ph.CO].
- [12] J. Garcia-Bellido and D. G. Figueroa, Phys. Rev. Lett. **98** (2007) 061302 doi:10.1103/PhysRevLett.98.061302 [astro-ph/0701014].
- [13] J. Garcia-Bellido, D. G. Figueroa and A. Sastre, Phys. Rev. D **77** (2008) 043517 doi:10.1103/PhysRevD.77.043517 [arXiv:0707.0839 [hep-ph]].
- [14] J. F. Dufaux, A. Bergman, G. N. Felder, L. Kofman and J. P. Uzan, Phys. Rev. D **76** (2007) 123517 doi:10.1103/PhysRevD.76.123517 [arXiv:0707.0875 [astro-ph]].
- [15] C. J. Hogan, Mon. Not. Roy. Astron. Soc. **218** (1986) 629.
- [16] G. N. Felder, J. Garcia-Bellido, P. B. Greene, L. Kofman, A. D. Linde and I. Tkachev, Phys. Rev. Lett. **87** (2001) 011601 doi:10.1103/PhysRevLett.87.011601 [hep-ph/0012142].
- [17] J. F. Dufaux, G. Felder, L. Kofman and O. Navros, JCAP **0903** (2009) 001 doi:10.1088/1475-7516/2009/03/001 [arXiv:0812.2917 [astro-ph]].
- [18] J. Garcia-Bellido, D. Y. Grigoriev, A. Kusenko and M. E. Shaposhnikov, Phys. Rev. D **60** (1999) 123504 doi:10.1103/PhysRevD.60.123504 [hep-ph/9902449].
- [19] L. M. Krauss and M. Trodden, Phys. Rev. Lett. **83** (1999) 1502 doi:10.1103/PhysRevLett.83.1502 [hep-ph/9902420].
- [20] E. J. Copeland, D. Lyth, A. Rajantie and M. Trodden, Phys. Rev. D **64** (2001) 043506 doi:10.1103/PhysRevD.64.043506 [hep-ph/0103231].
- [21] A. Tranberg and J. Smit, JHEP **0311** (2003) 016 doi:10.1088/1126-6708/2003/11/016 [hep-ph/0310342].
- [22] K. Enqvist, S. Nurmi, S. Rusak and D. Weir, JCAP **1602** (2016) no.02, 057 doi:10.1088/1475-7516/2016/02/057 [arXiv:1506.06895 [astro-ph.CO]].
- [23] J. Garcia-Bellido, M. Garcia Perez and A. Gonzalez-Arroyo, Phys. Rev. D **67** (2003) 103501 doi:10.1103/PhysRevD.67.103501 [hep-ph/0208228].
- [24] J. Smit and A. Tranberg, JHEP **0212** (2002) 020 doi:10.1088/1126-6708/2002/12/020 [hep-ph/0211243].
- [25] A. Arrizabalaga, J. Smit and A. Tranberg, JHEP **0410** (2004) 017 doi:10.1088/1126-6708/2004/10/017 [hep-ph/0409177].
- [26] Z. G. Mou, P. M. Saffin and A. Tranberg, In preparation.
- [27] J. I. Skullerud, J. Smit and A. Tranberg, JHEP **0308** (2003) 045 doi:10.1088/1126-6708/2003/08/045 [hep-ph/0307094].

- [28] J. Garcia-Bellido, M. Garcia-Perez and A. Gonzalez-Arroyo, Phys. Rev. D **69** (2004) 023504 doi:10.1103/PhysRevD.69.023504 [hep-ph/0304285].
- [29] J. Ghiglieri and M. Laine, JCAP **1507** (2015) no.07, 022 doi:10.1088/1475-7516/2015/07/022 [arXiv:1504.02569 [hep-ph]].